Carbon 137 (2018) 527–532

Contents lists available at ScienceDirect

Carbon

journal homepage: www.elsevier.com/locate/carbon

Mechanisms of elementary hydrogen ion-surface interactions during multilayer graphene etching at high surface temperature as a function of flux

D.U.B. Aussems [a, *], K.M. Bal [b], T.W. Morgan [a], M.C.M. van de Sanden [a, c], E.C. Neyts [b]

[a] DIFFER - Dutch Institute for Fundamental Energy Research, De Zaale 20, 5612 AJ, Eindhoven, the Netherlands
[b] University of Antwerp, Department of Chemistry, PLASMANT Research Group, Universiteitsplein 1, 2610 Antwerp, Belgium
[c] Eindhoven University of Technology, PO Box 513, 5600 MB, Eindhoven, the Netherlands

ARTICLE INFO

Article history:
Received 21 February 2018
Received in revised form
9 May 2018
Accepted 23 May 2018
Available online 24 May 2018

ABSTRACT

In order to optimize the plasma-synthesis and modification process of carbon nanomaterials for applications such as nanoelectronics and energy storage, a deeper understanding of fundamental hydrogen-graphite/graphene interactions is required. Atomistic simulations by Molecular Dynamics have proven to be indispensable to illuminate these phenomena. However, severe time-scale limitations restrict them to very fast processes such as reflection, while slow thermal processes such as surface diffusion and molecular desorption are commonly inaccessible. In this work, we could however reach these thermal processes for the first time at time-scales and surface temperatures (1000 K) similar to high-flux plasma exposure experiments during the simulation of multilayer graphene etching by 5 eV H ions. This was achieved by applying the Collective Variable-Driven Hyperdynamics biasing technique, which extended the inter-impact time over a range of six orders of magnitude, down to a more realistic ion-flux of 10^{23} $m^{-2}s^{-1}$. The results show that this not only causes a strong shift from predominant ion-to thermally-induced interactions, but also significantly affects the hydrogen uptake and surface evolution. This study thus elucidates H ion-graphite/graphene interaction mechanisms and stresses the importance of including long time-scales in atomistic simulations at high surface temperatures to understand the dynamics of the ion-surface system.

1. Introduction

Hydrogen-graphite/graphene interactions are relevant to a wide variety of applications, ranging from astrophysics [1], nuclear fusion [2–4], fuel cells [5,6], gas and energy storage [7–9], to nano-electronics [10–15]. For instance, they occur during the plasma-synthesis of carbon nanomaterial components that are used in some of these applications, such as (multilayer) graphene (MLG) [16–19] and carbon nanowalls (CNWs) [9,20]. An enormous amount of knowledge of these interaction phenomena was gained in fusion energy research, in which dedicated experiments were performed on tokamaks [21] and ion beam setups [22,23], in conjunction with development of theoretical models [4,24–27]. More recently, further insights into fundamental properties for adsorption, diffusion and desorption have been obtained by density function theory [28–36] and thermal desorption experiments using hot (~0.2 ev) H atom beam sources [37–39]. Generally, it is understood that exposure to H species (ionized or hot) entails a dynamics of hydrogenation on the one hand, and release of hydrogen through desorption and chemical and physical sputtering on the other hand [24,26].

Due to atomistic length scale of the ion-surface interaction, as well as the interconnected and cumulative nature of the various processes involved, it remained very challenging to verify the elementary mechanisms during the plasma exposure. For instance, it is unclear what factors influence recombinative H_2 desorption and to what extent diffusion-induced (Langmuir-Hinshelwood) H-H recombination can occur. In this regard, atomistic simulations using Molecular Dynamics (MD) can provide valuable insights, not only for the interaction of hydrogen ions with graphite/graphene at high surface temperature discussed in this work, but also for closely related materials such as amorphous-carbon coatings [40], carbon

* Corresponding author.
E-mail address: d.aussems@differ.nl (D.U.B. Aussems).

https://doi.org/10.1016/j.carbon.2018.05.051
0008-6223/

nanotubes (CNTs) [41–43], and nanocrystalline diamond [44].

With regards to common plasma processing of graphite/graphene, various elementary ion-surface processes were investigated by Despiau-Pujo et al. [16,17,45]. The results show that H ions can either reflect, adsorb or penetrate at the surface, and the probability for each process depends on the ion energy. In the case when a H ion is adsorbed, several additional processes can occur; it can be sputtered by a H ion impact with consecutive reflection of the impacting H ion, recombine straight with the incoming H ion (so called Eley-Rideal recombination), or recombine with another H atom at the surface [17]. Unfortunately, because of the severe time-scale limitation of MD, the typical inter-impact time in these simulations was very short (~1 ps) so that the resulting simulated ion-flux is higher by at least four orders of magnitude than any experiment. Long time-scale processes (of the order of μs–ms) that become important at elevated surface temperatures and low fluxes can thus not be accessed. Examples of these processes are: hydrogen surface diffusion [46], Langmuir-Hinshelwood recombination, desorption of hydrogen and weakly bound species [47], and other surface relaxation phenomena [48,49].

In order to reach these desirable longer time-scales of thermal processes, we have presented a simulation approach in our previous work [49]; the applications of a recently developed acceleration procedure, collective variable-driven hyperdynamics (CVHD) [50]. This is a generic implementation of the hyperdynamics method [51], in which the waiting time between minima-to-minima transitions is reduced by adding a bias potential (ΔV) to the global potential energy surface (PES) of the system. In CVHD, the bias potential is built on the fly and in a self-learning fashion. This allows the method - in contrast to other hyperdynamics implementation - to be more generically applicable while little system-specific optimization is required. In previous work, CVHD was applied to accelerate processes involving the breaking of C-C bonds in the graphite lattice. The increased inter-impact time enabled us to observe the transition from ion-to thermally-induced chemical sputtering at lower, more realistic fluxes. The detailed (thermal) behavior of hydrogen ions with the surface remained uncertain, however, because biasing was not applied to the C-H bonds.

In the work presented here, these elementary H ion-surface interactions are investigated in detail. First, a semi-empirical model is introduced to show under what conditions long time-scale thermal processes are important. Then, by applying the CVHD method with C-C/C-H bond biasing [50], the inter-impact time is extended towards a more relevant time-scale, i.e. from 3 ps up to 1 μs (a flux of 10^{23} $m^{-2}s^{-1}$). We will show that this has a significant impact on the type of ion-surface interactions, H uptake and surface evolution.

2. Semi-emprical model for ion-surface interactions

The type of hydrogen ion-surface interaction can be predicted using the semi-empirical Roth-Garcia-Rosales model [21,25,26] which was initially developed to describe the chemical sputtering of graphite. In this model the graphite surface is considered to experience a cycle of amorphization by hydrogenation (transforming sp^2 C atoms into sp^3 C) and recovery back into sp^2 C due to desorption of hydrogen and weakly bound hydrocarbon molecules (via intermediate radical state $sp^{x,1}$ C and $sp^{x,2}$ C). Using experimental data as input, the model can predict the chemical sputtering yield as function of various quantities such as the ion energy, ion-flux, isotope mass, surface temperature and surface state [4,21]. Yet, it can also be employed to predict the rate of various hydrogen release mechanisms, including recombinative desorption (with rate constant k_{-H}), ion-induced H release (with cross-section σ_D), and chemical sputtering (with rate coefficient k_x for thermally-induced erosion and cross-section σ_x for ion-induced erosion). The ratio of the ion-to thermally-induced hydrogen release rates can be determined by:

$$\beta = \frac{\sigma_D\varphi[sp^3] + \sigma_x\varphi[sp^3]}{k_{-H}[sp^{x,1}] + k_x[sp^{x,2}]} = \frac{(\sigma_D\varphi + \sigma_x\varphi)(k_x + \sigma_x\varphi)}{k_{-H}k_x\sigma_D/\sigma_H + k_x\sigma_D\varphi} \quad (1)$$

where φ is the H ion-flux and σ_H is the adsorption cross-section of the H ion. Based on Eq. (1), the surface temperature above which the thermally-induced interaction dominates ($\beta < 1/9$) and its transition zone ($1/9 < \beta < 9$, i.e., from 90% to 10% thermal processes) was plotted in Fig. 1. The typical ion-flux ranges for experiments are included as well, as are the typical conditions of other MD simulations. It shows that most MD simulations on graphite etching (hollow scatter points) are far outside the ion-flux range of plasma experiments by several orders of magnitude. Moreover, none of these simulation reached the thermally-induced regime, hence detailed investigation in this unexplored domain is required.

3. Simulation model

In our simulation we applied the conditions typical for applications that involve high-flux plasma exposure [55], e.g. nanostructuring of graphite surfaces [9] and erosion of tokamak walls made of graphite [21]. The typical high surface temperature of 1000 K enabled us to explore the transition towards thermal H-surface interactions. An elaborate description of the simulation method is provided in our previous article [49], and briefly summarized below. The simulations were performed using the LAMMPS package [56], and modified Colvars module [57]. The interatomic potential applied was the Reactive Force field (ReaxFF) [58] with the parameter set developed by Mueller et al. [59]. The plasma interaction with the graphite substrate was simulated by impacting the surface with 5 eV H atoms at random

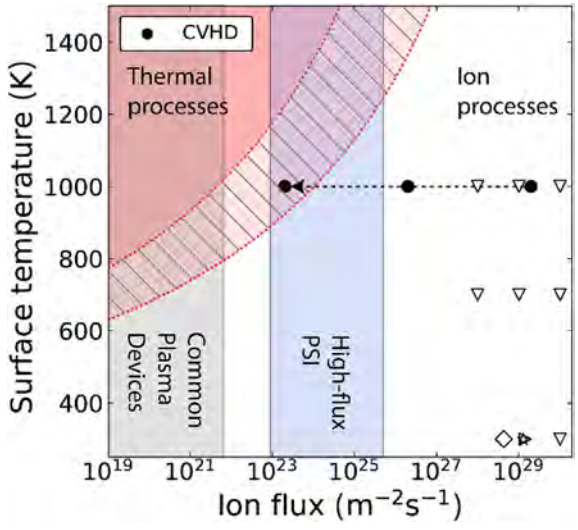

Fig. 1. Domains of predominant ion (blank area) and thermal (red area) hydrogen-surface processes as function of the ion-flux and surface temperature, including the transition region (marked area), as predicted by the Roth-Garcia-Rosales model [21,25]. The selected ion energy was 5 eV. The conditions of current CVHD simulation is depicted as well (●). For comparison, the data from previous MD simulations of H ion bombardment on a-C:H (▽ [52], ◇ [53], ▷ [54]) and graphite (★ [16,17]) are included, as are the typical flux ranges of common plasma and high-flux PSI devices [55]. (A colour version of this figure can be viewed online.)

(x,y) positions at normal incidence. The graphite substrate was composed of 4 graphene layers in ABAB stacking (size 20 Å × 20 Å, periodic x,y boundary conditions), which was initially brought to a temperature of 1000 K. After the H impact, the motion of each atom was followed for 1 ps in the micro-canonical (NVE) ensemble to capture the physics of the initial hydrogen impact. Hereafter, the natural heat conduction out of the cell was mimicked by a 1 ps canonical ensemble (NVT) phase, where the substrate was cooled to its original temperature by a Nosé-Hoover style thermostat [60].

Next, the full inter-impact time before the next impact (1 μs) was simulated by a CVHD phase, which is in contrast to other simulations where it is assumed that in this time nothing happens. In order to do this, the simulated physical time was elongated by multiplying the MD time (using 0.1 fs time step) by the boost factor $e^{\beta\Delta V}$, in which $\beta = 1/(k_B T)$ [51]. The CVHD bias ΔV was dynamically generated by adding small repulsive Gaussian potentials (width 0.04 and height 0.01 eV) to the local PES every 100 fs. The bias potential is a function of the distortion functions $(r_i - r_{min})/(r_{max} - r_{min})$ of all the C-C or C-H bond lengths r_i. We used $r_{max,CC} = 2.20$ Å, $r_{min,CC} = 1.50$ Å, $r_{max,CH} = 1.65$ Å and $r_{min,CH} = 1.05$ Å. In this way, a 6 order of magnitude increase of the simulated time was achieved, while the calculation time was only up to a factor 9 longer. In the 3 ps and 1 ns inter-impact case, 3000 impacts were simulated, while this was 1700 in the case of 1 μs inter-impact time.

After each CVHD phase a new impact was simulated (i.e. starting from the NVE phase). Once erosion was initiated and eroded species entered the removal zone, they were deleted from the simulation after each simulation phase (i.e. NVE, NVT, and CVHD).

4. Results

4.1. Short time-scale simulation

The evolution of the surface during ion bombardment was first simulated with an inter-impact time of only 3 ps, from which 1 ps was CVHD phase. Similarly to in Refs. [16,17] we observe the following interaction mechanisms (see Fig. 2): reflection, Eley-Rideal (E-R) recombination, H sputtering by H ion impact, H release through ion-induced hydrocarbon erosion and direct H_2 recombination of H atoms. The latter was not originally expected, but is plausible because of the large thermal vibrations of the H and C atoms at high surface temperatures. In contrast to Ref. [16,17], we find that in the case of H sputtering the incoming H ion can also chemisorb after impact rather than only reflect. Penetration through the graphene layer was negligible as its insignificant at 5 eV ion impact energy [45].

By determining the point when the H atom was released from the surface, the type of process and its probability could be estimated. The results are shown in Fig. 3. At a 3 ps inter-impact time, 17% of the incoming H ions were reflected. The remainder was chemisorbed on the surface. From these H atoms, a majority (64%) recombined by an Eley-Rideal process. Only a limited fraction (<19%) was released through surface recombination, H sputtering and erosion. Because the probability of the different interaction processes depended on the exact surface configuration, and thus the number of impacts, the surface evolution was examined by monitoring the uptake of H as well as hydrocarbon groups on the surface (Fig. 4a, top). Three phases could be identified. In phase I, the surface was quickly hydrogenated up a H uptake of 25, corresponding to a H concentration of ~20%, within 200 impacts. In phase II, hydrocarbon groups appeared on the surface, starting from CH_2 to eventually CH_3 groups after 500 impacts. Lastly, in phase III, after ~550 impacts etching was initiated and continued until ~1500 impacts, where nearly all carbon and hydrogen atoms in the first layer were released. The maximum H uptake was ~130, corresponding to a H concentration of ~110% (consistent with Ref. [16]). Concurrently, the same cycle is initiated for the underlying layer after the first holes appear in the top graphene layer (after ~1300 impacts).

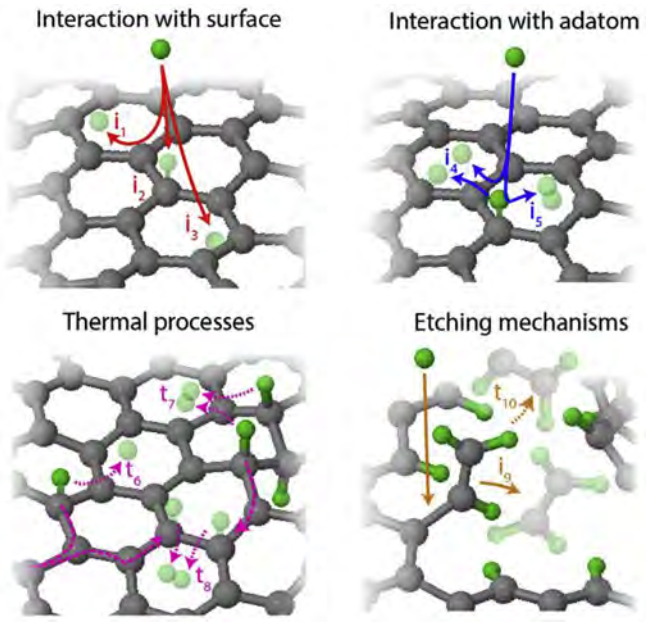

Fig. 2. Illustration of the H ion-surface interactions. The labels i_x and t_x reflect whether the interaction includes a thermally- or ion-induced process. At first, basic interaction with the surface can occur; the impinging H ions either i_1) reflects, i_2) chemisorbs on a surface C atom, or i_3) penetrates through the top graphene layer. If the H atom is chemisorbed, multiple other mechanisms can occur. A consecutive impacting H ion can i_4) sputter the H ad-atom or i_5) cause H_2 recombination (Eley-Rideal recombination). The chemisorbed H atoms can also be released thermally by t_6) H desorption, t_7) direct surface recombination, or t_8) diffusion-induced surface recombination (Langmuir-Hinshelwood recombination). Lastly, the H atom can be released due to chemical sputtering of a hydrocarbon group either induced by i_9) an ion-impact or t_{10}) thermal fluctuations. (A colour version of this figure can be viewed online.)

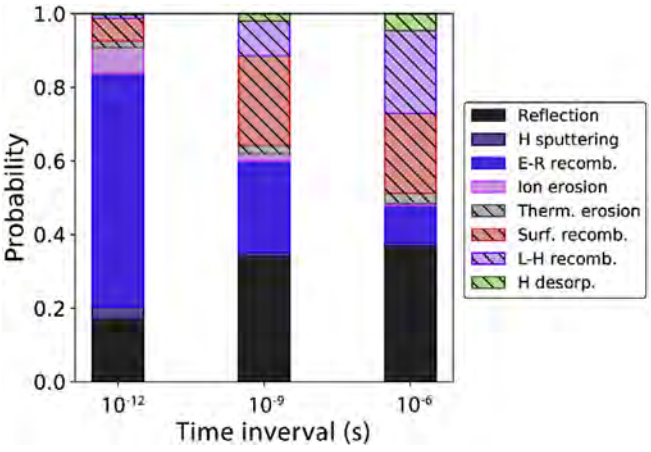

Fig. 3. The probability for hydrogen ion interactions with the surface: reflection (i_1), H sputtering (i_4), Eley-Rideal recombination (i_5), H desorption (t_6), surface recombination (t_7), Langmuir-Hinshelwood recombination (t_8), and ion- and thermally-induced erosion (i_9 and t_{10}), for varying inter-impact times: 3 ps, 1 ns and 1 μs. The thermal processes are marked with a line pattern. The probability was calculated based on the full fluence of the simulations (see Sec. 3).

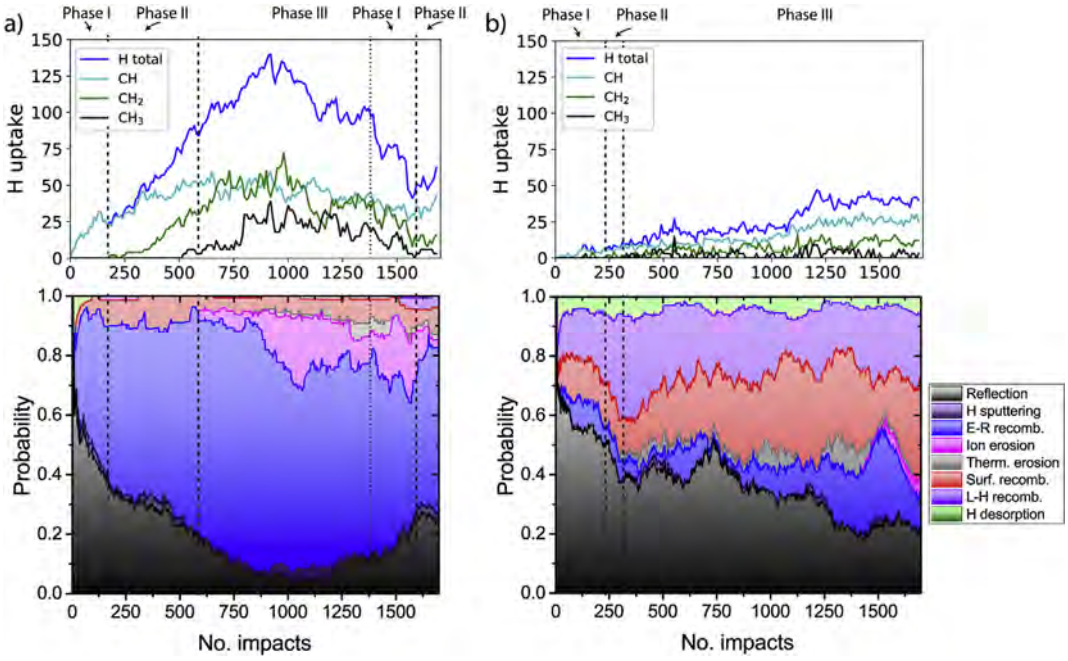

Fig. 4. Time evolution of (top) the total hydrogen uptake in the system and the present hydrogen in CH, CH_2 and CH_3 groups and (bottom) the probability for hydrogen ion interactions with the surface: reflection (i_1), H sputtering (i_4), Eley-Rideal recombination (i_5), H desorption (t_6), surface recombination (t_7), Langmuir-Hinshelwood recombination (t_8), and ion- and thermally-induced erosion (i_9 and t_{10}). Three phases were identified: low H uptake (Phase I), rise of complex hydrocarbon groups at the surface (Phase II) and start of chemical sputtering (Phase III). The inter-impact time interval was a) 3 ps and b) 1 μs.

By depicting the probability for each ion-surface process (averaged over 100 impacts) versus the number of impacts (Fig. 4a bottom), its correlation with the aforementioned erosion phases could be identified. The results show that initially in phase I, reflection was relatively high (~60%). This is in line with Ref. [45], where a 5 eV H ion energy was found to be close to the threshold for adsorption. Persistent bombardment of H ions, however, eventually led to significant hydrogenation in phase II, resulting in a reduced reflection probability (<30%). This can be explained by the rise of *ortho*- and *para*-sites (e.g. H clusters) [34] and defects [45], which both increase the effective binding energy. Hence, we note that in contrast to what is typically assumed, the adsorption behavior (see Fig. S1a in the supplementary information) is not Langmuirian, i.e. the adsorption cross-section cannot be expressed as $\sigma_H = s_H/n_0(1 - n_H/n_0)$, where s_H, n_H and n_0 are respectively the sticking coefficient of hydrogen ions, the H concentration (H uptake per surface area) and total density of surface sites [27]. In phase II, Eley-Rideal recombination became more dominant (>50%), which can be explained by the larger E-R cross-section for increasing H uptake. The same applies for the increase in H sputtering, although its contribution is relative small. In phase III, besides E-R recombination, a significant fraction (~30%) of H was released through ion-induced hydrocarbon etching, which evidently required a minimum H uptake before initiation.

4.2. Long-time-scale simulation

By moving towards more realistic time intervals, e.g. 1 μs, corresponding to an ion-flux of $10^{23}\,m^{-2}s^{-1}$, four new thermal processes occurred (see Fig. 2): thermally-induced hydrocarbon erosion (which was already discussed in Ref. [49]), surface diffusion, hydrogen desorption, and diffusion-induced Langmuir-Hinshelwood (L-H) recombination. The processes mutually competed: the chemisorbed H atoms either desorbed (as a single H atom or as H_2 by direct recombination with a neighboring H atoms), diffused to neighboring C atoms, or - if the H atom was not desorbed after several hopping events - encountered another H atom and recombined (L-H kinetics). N.b., to avoid confusion with surface recombination, we defined L-H recombination here as an event where both H atoms hopped at least once before recombining.

The probabilities for the ion-surface processes clearly altered due to the prolonged time interval between impacts, (Fig. 3). The reflection probability rose from 17 to 37%, which is related to both the uncompleted erosion cycle over which the impacts were averaged (resulting in overestimation of <10%) as well as the lower mean H uptake. Moreover, E-R recombination reduced with increasing inter-impact time, while direct surface recombination and Langmuir-Hinshelwood kinetics (Fig. 2) started to dominate. In the case of direct surface recombination this shift is related to the higher probability for C-H bond breaking (the rate limiting step). This is also the case for L-H recombination, but since it additionally involves a rate-limiting (2nd order) diffusion step, the increase is more pronounced. The prolonged inter-impact time also led to the rise of H desorption; from virtually 0–5%. Overall, the fraction of H release through thermal processes increased from 11 to 82%.

The consequence of the shift in competing interaction mechanisms is clearly visible in the evolution of the etching process for the 1 μs inter-impact time simulation (Fig. 4b). It is apparent that compared to the 3 ps inter-impact time simulation, hydrogenation is suppressed and does not exceed a H uptake of 50, which corresponds to a H concentration of ~40%, similar as found in experiments [24]. The reason for the drop in H uptake is that due to the extended inter-impact time, H atoms are more likely to desorb. This is surely the case for loosely bound H atoms and hydrocarbon molecules. Nevertheless, H atoms near defects and H clusters are able to continue being bound due to the higher binding energy. Despite the reduced H uptake, formation of weakly bound CH_3 groups and erosion are initiated after fewer impacts (after ~300 impacts for both cases, rather than ~500 and ~600, respectively). This can attributed to a similar mechanism as was found in previous work [49]: a higher probability for C-C bond breaking due to prolonged exposure to thermal stress resulted in more potential

binding sites [49] (this is also supported by the observed transition towards hydrocarbon release by thermally-induced C-C bond breaking, see Fig. S2 in the supplementary information).

Similarly to the ps-scale simulation, the probability of the ion-surface interactions strongly alter during the erosion cycle, mainly due to a changing H uptake. In the case of the ion-induced processes the trends were similar as described above. Direct surface recombination shows a strong increase with increasing H uptake (similar to E-R recombination and H sputtering), which is due to the higher probability to neighbor a binding partner. L-H recombination exhibits a clear optimum around 400 impacts (see also Fig. S1g in the supplementary information), at a H uptake of ~15. This may be attributed to two competing requirements: a minimum H uptake is necessary for the H atoms to find a recombination partner, while the uptake should not be exceedingly high, because then L-H kinetics is impeded by trapping at the defects and H clusters as well as by reduced mobility due to holes and disconnected carbon islands [49] (this is also supported by the rising surface residence time and dropping number of hopping events with increasing H uptake, see Fig. S3 in the supplementary information). Lastly, H desorption shows a decrease with H uptake, which can again be related to the stronger binding at defects and H clusters.

5. Discussion

Based on the semi-empirical Roth-Garcia-Rosales model, we predicted a shift from ion-to thermally-induced hydrogen graphite interaction. Fig. 3 shows that with our CVHD simulation we were able to reproduce the same trend; the contribution of thermally-induced interactions increased from 11 to 82% when the flux was reduced from 10^{29} to 10^{23} $m^{-2}s^{-1}$. The tipping point was, however, higher than expected (at a flux of ~10^{26} $m^{-2}s^{-1}$) and the transition region wider. This could be explained by limitations of the interatomic potential (resulting in deviating rate coefficients), but can also be related to factors which are not considered in the current work, such as the microscopic morphology. Nevertheless, the trend qualitatively agrees with the model.

The observed interactions observed in our work may lead to improved insight of the dynamics in related simulations at elevated surface temperatures. For instance, in the MD simulation on graphene patterning by hydrogen plasma (at a surface temperature of 570 K) [18,19], thermal processes are expected to be significant, but are not included. Based on our results, it is expected that the erosion cycle is not altered and still proceeds via the same phases (hydrogenation, CH_2/CH_3 group formation, and hydrocarbon etching); however, the shift towards thermal processes means that a significant fraction of the simulated processes – which drive this erosion cycle – cannot be captured and instead are replaced by ion-induced processes (e.g. recombinative desorption for E-R recombination). As a result, the hydrocarbon etching rate constant and H release rate are underestimated, while the hydrocarbon surface concentration is overestimated. This results in either an under- or overestimation of the erosion rate, depending on the relative magnitude of the latter competing effects. Lastly, the type of etching species can significantly vary, as was demonstrated in Ref. [49].

The atomistic nature of the CVHD simulation also allowed us to complement the knowledge behind the semi-empirical model by providing more detailed insights into the dynamics of the interactions. First of all, several interactions were found which were not explicitly mentioned in the literature on graphite etching: direct surface recombination, H desorption, surface diffusion, and L-H recombination. In the model, these processes are all incorporated in the rate coefficient for thermal H release (k_{-H}). This means that the selected activation energy for this rate is probably the mean value of a spectrum of energies. On a similar note, it was found that the ion-induced H release (σ_D) in the model not only involves E-R recombination, but also H sputtering. Lastly, the results show that the rate coefficients and cross-sections are not constant, but vary with time, i.e. over the three phases of the erosion cycle (see Fig. 4). More specifically, their value strongly depended on the H uptake, while the H uptake again was correlated to the rate of desorption. These mutual dependencies indicate that the detailed dynamics of the ion-surface system may be more complex than initially assumed.

6. Conclusion

This work shows that the type of elementary hydrogen-ion graphite surfaces interaction can alter significantly by extending the inter-impact time. In line with the semi-empirical model for graphite etching, a clear shift was observed from predominantly ion-induced H release mechanisms such as Eley-Rideal recombination and H sputtering, towards thermally-induced processes such as direct surface recombination, Langmuir-Hinshelwood recombination and H desorption. In fact, these latter processes could be reached at conditions – ion flux of 10^{23} $m^{-2}s^{-1}$, surface temperature of 1000 K and ion energy of 5 eV – similar to high-flux plasma exposure experiments for the first time using atomistic simulation, which enabled us to describe the more detailed dynamics of the system. Hence, this study demonstrates that long time-scale effects in ion-surface simulations can be important, and in contrast to what is typically assumed in literature these effects, may not be neglected, especially for low ion-flux, high surface temperatures simulations. The approach adopted in this work may also be used to investigate other ion-surface systems or the effects of specific processes such as diffusion, desorption and relaxation on the self-assembly of nanostructures in plasma.

Acknowledgements

DIFFER is part of the Netherlands Organisation for Scientific Research (NWO). K.M.B. is funded as PhD fellow (aspirant) of the FWO-Flanders (Fund for Scientific Research-Flanders), Grant 11V8915N. The computational resources and services used in this work were provided by the VSC (Flemish Supercomputer Center), funded by the FWO and the Flemish Government – department EWI.

Appendix A. Supplementary data

Supplementary data related to this article can be found at https://doi.org/10.1016/j.carbon.2018.05.051.

References

[1] V. Sidis, L. Jeloaica, A.G. Borisov, S.A. Deutscher, F. Combes, G. des Forêts, Molecular hydrogen in space, Cambridge Contemp. Astrophys. Ser (2000) 89–97.
[2] G. Federici, C.H. Skinner, J.N. Brooks, J.P. Coad, C. Grisolia, A.A. Haasz, et al., Plasma-material interactions in current tokamaks and their implications for next step fusion reactors, Nucl. Fusion 41 (2001) 1967.
[3] J. Roth, A. Kirschner, W. Bohmeyer, S. Brezinsek, A. Cambe, E. Casarotto, et al., Flux dependence of carbon erosion and implication for ITER, J. Nucl. Mater. 337–339 (2005) 970–974.
[4] B.V. Mech, A.A. Haasz, J.W. Davis, Model for the chemical erosion of graphite due to low-energy H+ and D+ impact, J. Appl. Phys. 84 (1998) 1655–1669.
[5] V. Tozzini, V. Pellegrini, Prospects for hydrogen storage in graphene, Phys. Chem. Chem. Phys. 15 (2013) 80–89.
[6] B.H. Kim, S.J. Hong, S.J. Baek, H.Y. Jeong, N. Park, M. Lee, et al., N-type graphene induced by dissociative H2 adsorption at room temperature, Sci. Rep. 2 (2012) 690.
[7] G. Garberoglio, N.M. Pugno, S. Taioli, Gas adsorption and separation in realistic and idealized frameworks of organic pillared graphene: a comparative study,

J. Phys. Chem. C 119 (2015) 1980–1987.
[8] R. Kumar, V.M. Suresh, T.K. Maji, C.N.R.N.R. Rao, Porous graphene frameworks pillared by organic linkers with tunable surface area and gas storage properties, Chem. Commun. 50 (2014) 2015–2017.
[9] D.U.B. Aussems, K. Bystrov, İ. Doğan, C. Arnas, M. Cabié, T. Neisius, et al., Fast nanostructured carbon microparticle synthesis by one-step high-flux plasma processing, Carbon 124 (2017) 403–414.
[10] Y. Awano, Graphene for VLSI: FET and interconnect applications, in: Tech. Dig. - Int. Electron Devices Meet, IEDM, 2009.
[11] X. Hong, A. Posadas, K. Zou, C.H. Ahn, J. Zhu, High-mobility few-layer graphene field effect transistors fabricated on epitaxial ferroelectric gate oxides, Phys. Rev. Lett. 102 (2009), 136808.
[12] A.N. Pal, A. Ghosh, Ultralow noise field-effect transistor from multilayer graphene, Appl. Phys. Lett. 95 (2009) 82105.
[13] C.-J. Shih, A. Vijayaraghavan, R. Krishnan, R. Sharma, J.-H. Han, M.-H. Ham, et al., Bi- and trilayer graphene solutions, Nat. Nanotechnol. 6 (2011) 439–445.
[14] D. Haberer, L. Petaccia, M. Farjam, S. Taioli, S.A. Jafari, A. Nefedov, et al., Direct observation of a dispersionless impurity band in hydrogenated graphene, Phys. Rev. B 83 (2011), 165433.
[15] D. Haberer, D.V. Vyalikh, S. Taioli, B. Dora, M. Farjam, J. Fink, et al., Tunable band gap in hydrogenated quasi-free-standing graphene, Nano Lett. 10 (2010) 3360–3366.
[16] E. Despiau-Pujo, A. Davydova, G. Cunge, D.B. Graves, Hydrogen plasmas processing of graphene surfaces, Plasma Chem. Plasma Process. 36 (2016) 213–229.
[17] A. Davydova, E. Despiau-Pujo, G. Cunge, D.B. Graves, H+ ion-induced damage and etching of multilayer graphene in H2 plasmas, J. Appl. Phys. 121 (2017), 133301.
[18] A. Harpale, H.B. Chew, Hydrogen-plasma patterning of multilayer graphene: mechanisms and modeling, Carbon 117 (2017) 82–91.
[19] A. Harpale, M. Panesi, H.B. Chew, Plasma-graphene interaction and its effects on nanoscale patterning, Phys. Rev. B 93 (2016) 1–10.
[20] M. Hiramatsu, M. Hori, Carbon Nanowalls: Synthesis and Emerging Applications, Springer Science & Business Media, New York, 2010.
[21] J. Roth, R. Preuss, W. Bohmeyer, S. Brezinsek, A. Cambe, E. Casarotto, et al., Flux dependence of carbon chemical erosion by deuterium ions, Nucl. Fusion 44 (2004) L21–L25.
[22] B.V. Mech, A.A. Haasz, J.W. Davis, Chemical erosion of pyrolytic graphite by low-energy H+ and D+ impact, J. Nucl. Mater. 241–243 (1997) 1147–1151.
[23] B.V. Mech, A.A. Haasz, J.W. Davis, Isotopic effects in hydrocarbon formation due to low-energy H+/D+ impact on graphite, J. Nucl. Mater. 255 (1998) 153–164.
[24] J. Küppers, The hydrogen surface chemistry of carbon as a plasma facing material, Surf. Sci. Rep. 22 (1995) 249–321.
[25] J. Roth, C. Garcia-Rosales, Analytic description of the chemical erosion of graphite by hydrogen ions, Nucl. Fusion 36 (1996) 1647–1659.
[26] A. Horn, A. Schenk, J. Biener, B. Winter, C. Lutterloh, M. Wittmann, et al., H atom impact induced chemical erosion reaction at C: H film surfaces, Chem. Phys. Lett. 231 (1994) 193–198.
[27] G. Federici, C.H. Wu, Modelling of the interaction of hydrogen plasma with amorphous carbon films redeposited in fusion devices, J. Nucl. Mater. 207 (1993) 62–85.
[28] L.F. Huang, M.Y. Ni, G.R. Zhang, W.H. Zhou, Y.G. Li, X.H. Zheng, et al., Modulation of the thermodynamic, kinetic, and magnetic properties of the hydrogen monomer on graphene by charge doping, J. Chem. Phys. 135 (2011) 64705.
[29] S. Casolo, O.M. Lovvik, R. Martinazzo, G.F. Tantardini, Understanding adsorption of hydrogen atoms on graphene, J. Chem. Phys. 130 (2009) 54704.
[30] S. Casolo, G.F. Tantardini, R. Martinazzo, Hydrogen recombination and dimer formation on graphite from ab initio molecular dynamics simulations, J. Phys. Chem. 120 (2016) 5032–5040.
[31] M. Kayanuma, U. Nagashima, H. Nishihara, T. Kyotani, H. Ogawa, Adsorption and diffusion of atomic hydrogen on a curved surface of microporous carbon: a theoretical study, Chem. Phys. Lett. 495 (2010) 251–255.
[32] K. Young-Kyun, Hydrogen adsorption on sp2-bonded carbon structures: Ab-initio study, J. Kor. Phys. Soc. 57 (2010) 778–786.
[33] V.V. Ivanovskaya, A. Zobelli, D. Teillet-Billy, N. Rougeau, V. Sidis, P.R. Briddon, Hydrogen adsorption on graphene: a first principles study, Eur. Phys. J. B. 76 (2010) 481–486.
[34] J. Kerwin, B. Jackson, The sticking of H and D atoms on a graphite (0001) surface: the effects of coverage and energy dissipation, J. Chem. Phys. 128 (2008) 84702.
[35] L. Hornekær, E. Rauls, W. Xu, Ž. Šljivančanin, R. Otero, I. Stensgaard, et al., Clustering of chemisorbed H(D) atoms on the graphite (0001) surface due to preferential sticking, Phys. Rev. Lett. 97 (2006), 186102.
[36] L. Hornekær, Ž. Šljivančanin, W. Xu, R. Otero, E. Rauls, I. Stensgaard, et al., Metastable structures and recombination pathways for atomic hydrogen on the graphite (0001) surface, Phys. Rev. Lett. 96 (2006), 156104.
[37] T. Zecho, A. Güttler, X. Sha, B. Jackson, J. Küppers, Adsorption of hydrogen and deuterium atoms on the (0001) graphite surface, J. Chem. Phys. 117 (2002) 8486–8492.
[38] T. Zecho, A. Güttler, J. Küppers, A TDS study of D adsorption on terraces and terrace edges of graphite (0001) surfaces, Carbon 42 (2004) 609–617.
[39] S. Baouche, G. Gamborg, V.V. Petrunin, A.C. Luntz, A. Baurichter, L. Hornekær, High translational energy release in H2 (D2) associative desorption from H (D) chemisorbed on C(0001), J. Chem. Phys. 125 (2006) 84712.
[40] E. Neyts, A. Bogaerts, M.C.M. Van De Sanden, Effect of hydrogen on the growth of thin hydrogenated amorphous carbon films from thermal energy radicals, Appl. Phys. Lett. 88 (2006), 141922.
[41] U. Khalilov, A. Bogaerts, B. Xu, T. Kato, T. Kaneko, E.C. Neyts, How the alignment of adsorbed ortho H pairs determines the onset of selective carbon nanotube etching, Nanoscale 9 (2017) 1653–1661.
[42] U. Khalilov, A. Bogaerts, E.C. Neyts, Atomic-scale mechanisms of plasma-assisted elimination of nascent base-grown carbon nanotubes, Carbon 118 (2017) 452–457.
[43] U. Khalilov, A. Bogaerts, S. Hussain, E. Kovacevic, P. Brault, C. Boulmer-Leborgne, et al., Nanoscale mechanisms of CNT growth and etching in plasma environment, J. Phys. D Appl. Phys. 50 (2017), 184001.
[44] M. Eckert, E. Neyts, A. Bogaerts, Molecular dynamics simulations of the sticking and etch behavior of various growth species of (Ultra) Nanocrystalline diamond films, Chem. Vap. Depos. 14 (2008) 213–223.
[45] E. Despiau-Pujo, A. Davydova, G. Cunge, L. Delfour, L. Magaud, D.B. Graves, Elementary processes of H2 plasma-graphene interaction: a combined molecular dynamics and density functional theory study, J. Appl. Phys. 113 (2013), 114302.
[46] V.A. Borodin, T.T. Vehviläinen, M.G. Ganchenkova, R.M. Nieminen, Hydrogen transport on graphene: competition of mobility and desorption, Phys. Rev. B 84 (2011) 75486.
[47] Y. Xia, Z. Li, H.J. Kreuzer, Adsorption, diffusion and desorption of hydrogen on graphene, Surf. Sci. 605 (2011) L70–L73.
[48] E.C. Neyts, A.C.T. Van Duin, A. Bogaerts, Changing chirality during single-walled carbon nanotube growth: a reactive molecular dynamics/Monte Carlo study, J. Am. Chem. Soc. 133 (2011) 17225–17231.
[49] D.U.B. Aussems, K.M. Bal, T.W. Morgan, M.C.M. Van De Sanden, E.C. Neyts, Atomistic simulations of graphite etching at realistic time scales, Chem. Sci. 8 (2017) 7160–7168.
[50] K.M. Bal, E.C. Neyts, Merging metadynamics into hyperdynamics: accelerated molecular simulations reaching time scales from microseconds to seconds, J. Chem. Theor. Comput. 11 (2015) 4545–4554.
[51] A.F. Voter, A method for accelerating the molecular dynamics simulation of infrequent events, J. Chem. Phys. 106 (1997) 4665–4677.
[52] E.D. de Rooij, U. von Toussaint, a W. Kleyn, W.J. Goedheer, Molecular dynamics simulations of amorphous hydrogenated carbon under high hydrogen fluxes, Phys. Chem. Chem. Phys. 11 (2009) 9823–9830.
[53] E. Salonen, K. Nordlund, J. Keinonen, C.H. Wu, Carbon erosion mechanisms in tokamak divertor materials: insight from molecular dynamics simulations, J. Nucl. Mater. 290–293 (2001) 144–147.
[54] P. Träskelin, K. Nordlund, J. Keinonen, H, He, Ne, Ar-bombardment of amorphous hydrocarbon structures, J. Nucl. Mater. 357 (2006) 1–8.
[55] G. De Temmerman, K. Bystrov, F. Liu, W. Liu, T. Morgan, I. Tanyeli, et al., Plasma – surface interactions under high heat and particle fluxes, Acta Polytech 53 (2013) 142–147.
[56] S. Plimpton, Fast parallel algorithms for short – range molecular dynamics, J. Comput. Phys. 117 (1995) 1–19.
[57] G. Fiorin, J. Hénin, New developments in the collective variables module: more flexible, more interactive, Biophys. J. 108 (2015) 160a.
[58] A.C.T. van Duin, S. Dasgupta, F. Lorant, G.W. A, ReaxFF: a reactive force field for hydrocarbonds, J. Phys. Chem. 105 (2001) 9396–9409.
[59] J.E. Mueller, A.C.T. Van Duin, W.A. Goddard, Application of the ReaxFF reactive force field to reactive dynamics of hydrocarbon chemisorption and decomposition, J. Phys. Chem. C 114 (2010) 5675–5685.
[60] G.J. Martyna, M.L. Klein, M. Tuckerman, Nosé-Hoover chains: the canonical ensemble via continuous dynamics, J. Chem. Phys. 97 (1992) 2635–2643.